Primary and secondary redox reactions

Here we present a few redox reactions represented by the RTM that are important in terms of TA dynamics and buffering capacity. A more complete description of sediment reactions is available in the supplementary material by Reed et al. (2016). Organic material (OM) in the reactions below is defined as $(CH_2O)_a(NH_3)_b(H_3PO_4)_c$, where a:b:c defines the molar C:N:P ratios for OM (e.g. C:N:P = 106:16:1). $\lambda \approx 0.18$ is the P:Fe ratio for iron-bound phosphorus (Reed et al., 2016).

TA and DIC are defined according to:

$$TA = [HCO_3^-] + 2[CO_3^=] + [HPO_4^=] + 2[PO_4^{3-}] + [NH_3] + [HS^-] - [H^+]$$

$$DIC = [CO_2^*] + [HCO_3^-] + [CO_3^=]$$

where

$$[CO_2^*] = [CO_2(aq)] + [H_2CO_3]$$

Primary redox reactions (all implemented in the RTM) and changes in TA and DIC (ΔTA and ΔDIC)

S1. Aerobic mineralization; ΔTA = b – c; ΔDIC = a.

- $OM + aO_2 \longrightarrow aCO_2 + aH_2O + bNH_3 + c(H_2PO_4^- + H^+)$

S2. Denitrification; ΔTA = 0.8a + b – c; ΔDIC = a.

- $OM + \frac{4a}{5}NO_3^- \longrightarrow \frac{a}{5}CO_2 + \frac{4a}{5}HCO_3^- + \frac{3a}{5}H_2O + \frac{2a}{5}N_2 + bNH_3 + c(H_2PO_4^- + H^+)$

S3. Manganese oxide (MnO_2) reduction; ΔTA = 4a + b – c; ΔDIC = a.

- $OM + 2aMnO_2 + 3aCO_2 + aH_2O \longrightarrow 4aHCO_3^- + 2aMn^{2+} + bNH_3 + c(H_2PO_4^- + H^+)$

S4. Iron oxyhydroxide ($Fe(OH)_3$) reduction; ΔTA = 8a + b – c + 4aλ; ΔDIC = a.

- $OM + 4a\{Fe(OH)_3 - \lambda HPO_4^=\} + 7aCO_2 \longrightarrow 8aHCO_3^- + 3aH_2O + 4aFe^{2+} + bNH_3 + c(H_2PO_4^- + H^+) + 4a\lambda HPO_4^=$

S5. Sulfate ($SO_4^=$) reduction; ΔTA = a + b – c; ΔDIC = a.

- $OM + \frac{a}{2}SO_4^= \longrightarrow aHCO_3^- + \frac{a}{2}H_2S + bNH_3 + c(H_2PO_4^- + H^+)$

S6. Methanogenesis; ΔTA = b – c; ΔDIC = 0.5a.

- $OM \longrightarrow \frac{a}{2}CO_2 + \frac{a}{2}CH_4 + bNH_3 + c(H_2PO_4^- + H^+)$

Secondary redox reactions implemented in the RTM and changes in TA and DIC (ΔTA and ΔDIC)

S7. Nitrification; ΔTA = -2; ΔDIC = 0.

- $2O_2 + NH_4^+ + 2HCO_3^- \longrightarrow NO_3^- + 2CO_2 + 3H_2O$

S8. Manganese re-oxidation; ΔTA = -4; ΔDIC = 0.

- $O_2 + 2Mn^{2+} + 4HCO_3^- \longrightarrow 2MnO_2 + 4CO_2 + 2H_2O$

S9. Iron re-oxidation; ΔTA = -8 - 4λ; ΔDIC = 0.

- $O_2 + 4Fe^{2+} + 8HCO_3^- + 2H_2O + 4\lambda HPO_4^= \longrightarrow 4\{Fe(OH)_3 - \lambda HPO_4^=\} + 8CO_2$

S10. Iron monosulfide (FeS) re-oxidation; ΔTA = 0; ΔDIC = 0.

- $2O_2 + FeS \longrightarrow SO_4^= + Fe^{2+}$

S11. Pyrite re-oxidation; ΔTA = -4; ΔDIC = 0.

- $7O_2 + FeS_2 + 2H_2O \longrightarrow 4SO_4^= + 2Fe^{2+} + 4H^+$

S12. Dissolved sulfide (H_2S) re-oxidation; ΔTA = -2; ΔDIC = 0.

- $2O_2 + H_2S + 2HCO_3^- \longrightarrow SO_4^= + 2CO_2 + 2H_2O$

S13. Aerobic methane oxidation; ΔTA = 0; ΔDIC = 1.

- $2O_2 + CH_4 \longrightarrow CO_2 + 2H_2O$

S14. Iron re-oxidation coupled to manganese oxide reduction; ΔTA = -2 - 2λ; ΔDIC = 0.

- $MnO_2 + 2Fe^{2+} + 2\lambda HPO_4^= + 2H_2O + 2HCO_3^- \longrightarrow 2\{Fe(OH)_3 - \lambda HPO_4^=\} + Mn^{2+} + 2CO_2$

S15. Manganese oxide reduction using dissolved sulfide; ΔTA = 2; ΔDIC = 0.

- $MnO_2 + H_2S + 2CO_2 \longrightarrow Mn^{2+} + S_0 + 2HCO_3^-$

S16. Iron oxyhydroxide reduction using dissolved sulfide; ΔTA = 4 + 2λ; ΔDIC = 0.

- $2\{Fe(OH)_3 - \lambda HPO_4^=\} + H_2S + 4CO_2 \longrightarrow 2Fe^{2+} + 2\lambda HPO_4^= + S_0 + 4HCO_3^- + 2H_2O$

S17. Iron monosulfide (FeS) formation; ΔTA = -2; ΔDIC = 0.

- $Fe^{2+} + H_2S + 2HCO_3^- \longrightarrow FeS + 2H_2O + 2CO_2$

S18. Anaerobic CH_4 oxidation by $SO_4^=$ reduction; ΔTA = 2; ΔDIC = 1.

- $SO_4^= + CH_4 + CO_2 \longrightarrow 2HCO_3^- + H_2S$

S19. Elemental sulfur disproportionation; ΔTA = -2; ΔDIC = 0.

- $S_0 + 4H_2O \longrightarrow 3H_2S + SO_4^= + 2H^+$

S20. Pyrite (FeS_2) formation using dissolved sulfide; ΔTA = 0; ΔDIC = 0.

- $FeS + H_2S \longrightarrow FeS_2 + H_2$

S21. Pyrite (FeS_2) formation using elemental sulfur; $\Delta TA = 0$; $\Delta DIC = 0$.

- $FeS + S_0 \longrightarrow FeS_2$

S22. Vivianite ($Fe_3(PO_4)_2 \cdot 8H_2O$) formation; $\Delta TA = -4$; $\Delta DIC = 0$.

- $3Fe^{2+} + 2HPO_4^{=} + 8H_2O \longrightarrow Fe_3(PO_4)_2 \cdot 8H_2O + 2H^+$

Tables and figures

Table S1. Equilibrium constants and associated equations for pH-dependent species.

Parameter	Equation K-value	Reference K-value
K_{CO_2}	$\frac{[HCO_3^-][H^+]}{[CO_2(aq)]}$	Millero et al. (2006)
$K_{HCO_3^-}$	$\frac{[CO_3^{2-}][H^+]}{[HCO_3^-]}$	Millero et al. (2006)
$K_{NH_4^+}$	$\frac{[NH_3][H^+]}{[NH_4^+]}$	Millero et al. (1995)
$K_{H_2PO_4^-}$	$\frac{[HPO_4^=][H^+]}{[H_2PO_4^-]}$	Millero et al. (1995)
$K_{HPO_4^=}$	$\frac{[PO_4^{3-}][H^+]}{[HPO_4^=]}$	Millero et al. (1995)
K_{H_2S}	$\frac{[HS^-][H^+]}{[H_2S]}$	Löffler et al. (2011)

Table S2. Pore water DIC and TA data (both in mM) measured at site F80 in June 2016.

Depth (cm)	DIC (mM)	TA (mM)
0	1.8	2.2
0.25	2.2	2.3
0.75	2.3	2.8
1.25	3.0	3.3
1.75	3.5	3.9
2.5	4.3	4.7
3.4	4.7	5.2
4.5	5.5	5.8
5.5	6.0	6.3
6.5	6.5	6.8
7.5	7.2	7.4
8.5	8.0	8.3
9.5	8.5	8.6
11	9.3	9.3
13	10.2	10.0
15	11.2	11.2
17	12.0	11.7
19	12.7	12.2
22	13.4	13.3
26	14.4	13.7
30	15.8	15.8
34	16.8	16.8
38	17.4	17.9
42	17.5	17.6
45.5	18.3	17.9

Table S3. Depth-integrated reaction rates of all processes involved in the S solids cycle at F80, as well as total formation rates for each of the three S solid species (all in mmol S m^{-2} y^{-1}). Negative numbers indicate a net loss of this species.

Rates (all in mmol S m^{-2} y^{-1})						
Period	FeS from $\sum H_2S$ and Fe^{2+}	FeS_2 from FeS and S^0	FeS_2 from FeS and $\sum H_2S$	S^0 from MnO_2 and $\sum H_2S$	S^0 from $Fe(OH)_3$ and $\sum H_2S$	FeS re-oxidation
1970-1973	19	7.1	12	6.5	8.0	0.01
1973-1978	65	24	37	5.5	25	0.02
1978-1981	283	73	182	0.82	76	0.06
1981-2009	73	36	39	0.49	42	0.00
Average	82	34	47	1.7	39	0.01

Period	FeS_2 re-oxidation	S^0 dispro-portionation	Total FeS_2 formation	Total FeS formation	Total S^0 formation	Total S solid formation
1970-1973	0.00	1.87	137	0.00	-0.06	37
1973-1978	0.12	1.82	120	5.2	-0.08	125
1978-1981	0.11	0.77	512	27	-0.14	539
1981-2009	0.00	1.63	151	-2.3	-0.05	148
Average	0.02	1.61	163	1.1	-0.06	164

Table S4. Observed linear TA-salinity relations for the mixing of Baltic Proper and Kattegat waters.

Year	Observed TA-salinity relation	Reference
1957	TA = 48S + 1128 (µmol kg^{-1})	Gripenberg (1960)[1]
1986	TA = 31S + 1270 (µmol kg^{-1})	Ohlson and Anderson (1990)
2000-2004	TA = 29.2S + 1417 (µmol l^{-1})	Perttilä et al. (2006)
2008	TA = 25.3S + 1470 (µmol kg^{-1})	Beldowski et al. (2010)

1. Calculated by Dyrssen (1993).

Table S5. Observed linear TA-salinity relations for the mixing of Baltic Proper and Gulf of Bothnia waters.

Year	Observed TA-salinity relation	Reference
1927-1935	TA = 179S + 274 (µmol l^{-1})	Based on Buch (1945)
1957	TA = 180S + 177 (µmol kg^{-1})	Gripenberg (1960)[1]
1986	TA = 177S + 139 (µmol kg^{-1})	Ohlson and Anderson (1990)
2000-2004	TA = 223S + 89.7 (µmol l^{-1})	Perttilä et al. (2006)
2008	TA = 205S + 229 (µmol kg^{-1})	Beldowski et al. (2010)

1. Calculated by Dyrssen (1993).

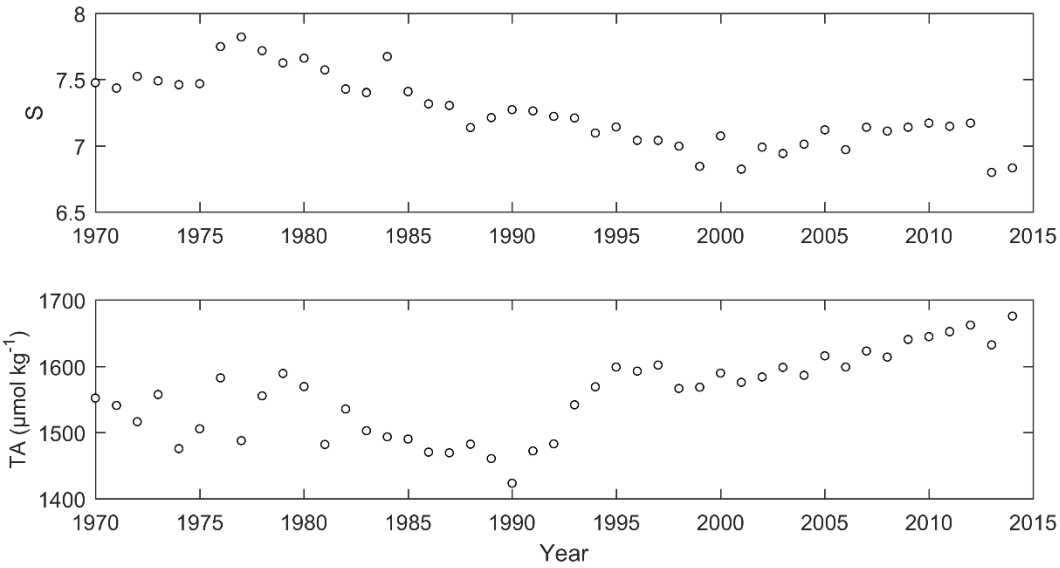

Figure S1. Annual mean observed surface water salinity and TA at the BY15 station in the Gotland Sea.

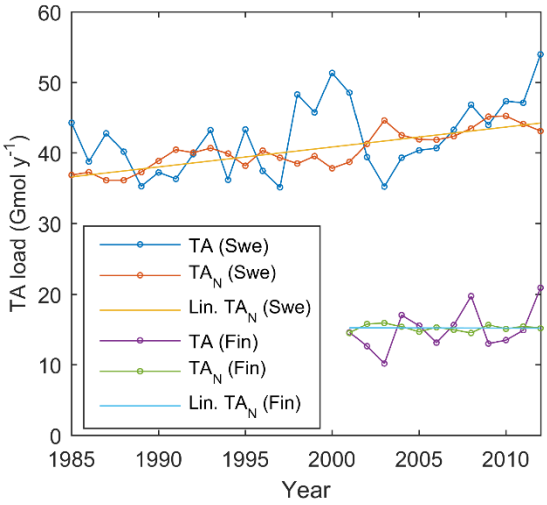

Figure S2. Observed riverine TA loads, flow normalized TA loads (TA_N) (Gmol y^{-1}), and linear trends (Lin. TA_N) in Swedish (Swe) and Finish (Fin) rivers respectively.

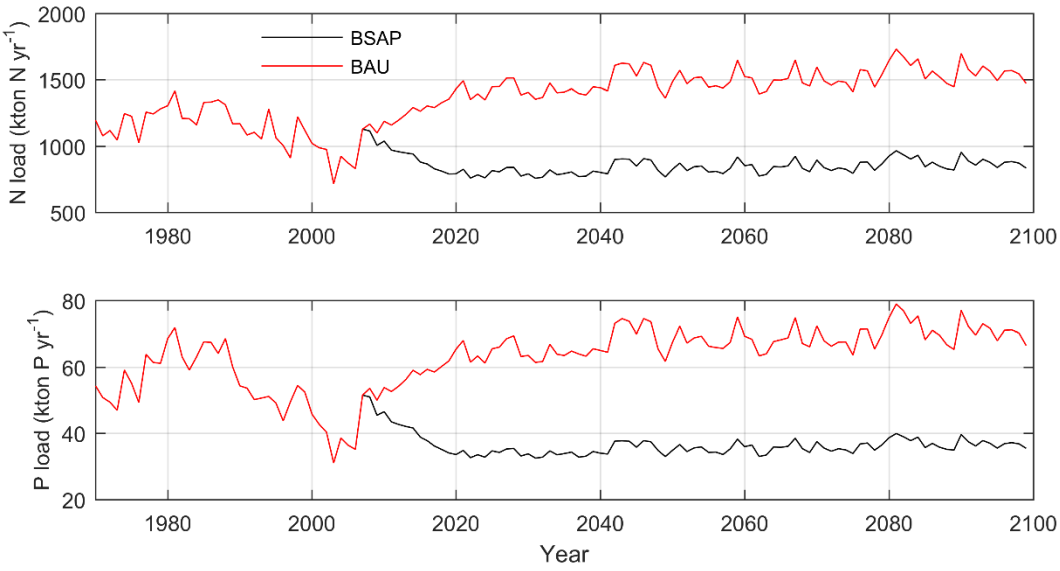

Figure S3. Nitrogen and phosphorus loads (land loads + atmospheric depositions) according to the BSAP and BAU scenarios respectively.

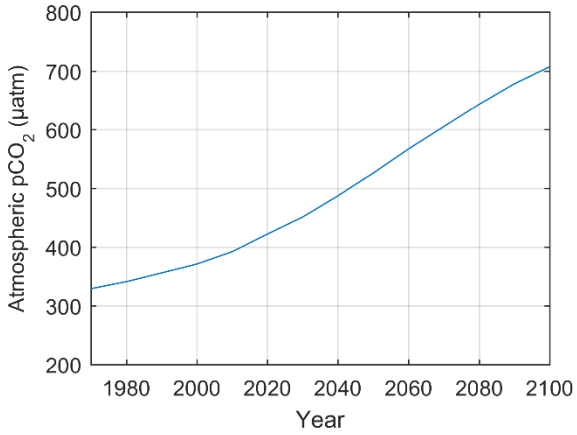

Figure S4. Annual mean atmospheric CO_2 partial pressure (pCO_2) according to the A1B emission scenario.

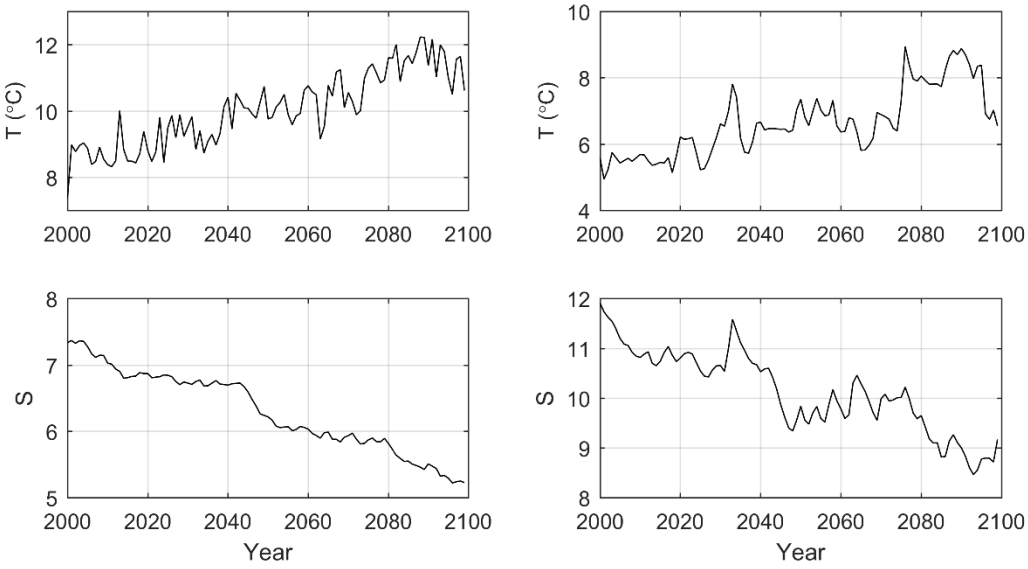

Figure S5. Simulated annual mean surface water (left) and deep water (right) temperature and salinity in the Gotland Sea.

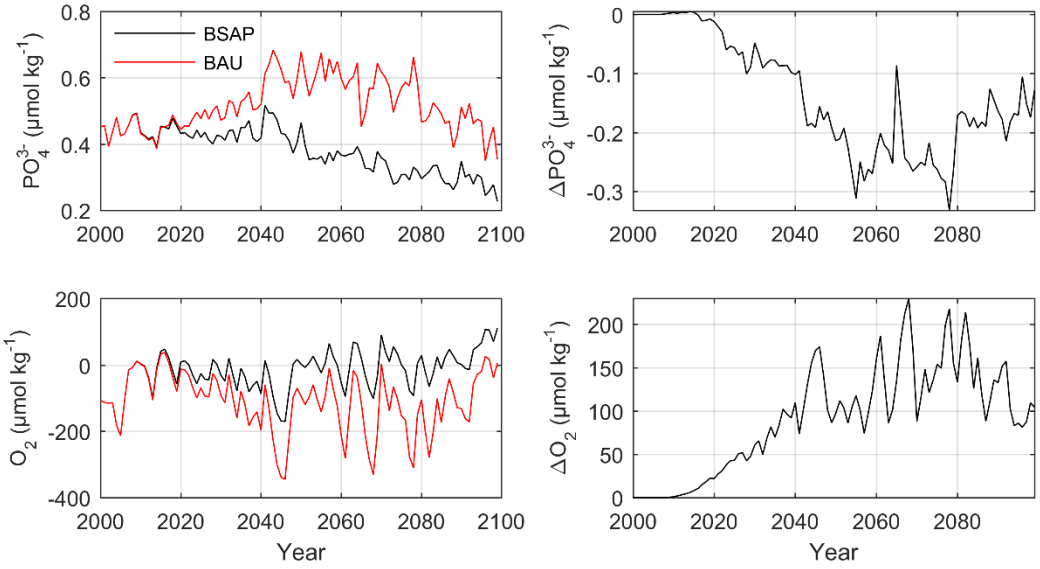

Figure S6. Left: simulated annual mean surface water phosphate and deep water oxygen concentrations in the Gotland Sea according to the BSAP (black lines) and BAU (red lines) nutrient load scenarios respectively. Right: differences between the BSAP and BAU scenarios.

References

Löffler, A., Schneider, B., Schmidt, M., Nausch, G., 2011. Estimation of denitrification in Baltic Sea deep water from gas tension measurements. Mar. Chem., 125, 91–100, doi:10.1016/j.marchem.2011.02.006.

Millero, F.J., 1995. Thermodynamics of the carbon dioxide system in the oceans. Geochim. Cosmochim. Ac., 59, 661–677, doi:10.1016/0016-7037(94)00354-O.

Millero, F.J., Graham, T.B., Huang, F., Bustos-Serrano, H., Pierrot, D., 2006. Dissociation constants of carbonic acid in seawater as a function of salinity and temperature. Mar. Chem., 100, 80–94, doi:10.1016/j.marchem.2005.12.001.

Reed, D.C., Gustafsson, B.G., Slomp, C.P., 2016. Shelf-to-basin iron shuttling enhances vivianite formation in deep Baltic Sea sediments. Earth Planet. Sci. Lett., 434, 241–251, doi:10.1016/j.epsl.2015.11.033.